

Cong Luo<sup>1,2</sup>  
Qiuwan Shen<sup>1</sup>  
Ning Ding<sup>1</sup>  
Zhixiang Feng<sup>3</sup>  
Ying Zheng<sup>1</sup>  
Chuguang Zheng<sup>1</sup>

Research Article

# Morphological Changes of Pure Micro- and Nano-Sized CaCO<sub>3</sub> during a Calcium Looping Cycle for CO<sub>2</sub> Capture

<sup>1</sup> State Key Laboratory of Coal Combustion, Huazhong University of Science and Technology, Wuhan, China.

<sup>2</sup> School of Mechanical and Mining Engineering, The University of Queensland, St. Lucia, Queensland, Australia.

<sup>3</sup> China United Engineering Corporation, Hangzhou, China.

Cyclic CO<sub>2</sub> capture using CaO-based sorbents derived from commercial pure micro-sized CaCO<sub>3</sub> and nano-sized CaCO<sub>3</sub> was investigated, focusing on the different characteristics of carbonation conversions, carbonation rates, surface areas, pore volumes, morphological changes, and microstrains of two sorbents during high-temperature reactions. The results indicated that the CaO-based sorbent derived from nano-sized CaCO<sub>3</sub> (NC-CaO) provided higher carbonation conversions and carbonation rates than the CaO-based sorbent derived from micro-sized CaCO<sub>3</sub> (MC-CaO) in the cyclic CO<sub>2</sub> capture reactions. Furthermore, NC-CaO retained its fast carbonation rate at the beginning of each cycle for several tens of seconds. In contrast, the carbonation rate of MC-CaO diminished with an increase in the cycle number. Unfortunately, NC-CaO sintered more easily. Its grains, which were composed of numerous spherical nanocrystallites, suffered from dramatic morphological changes during high-temperature reactions. A mechanism of grain boundary migration was employed to explain the sintering of CaO-based sorbent. The smaller crystallites were more susceptible to be merged by the bigger crystallites during high-temperature reactions.

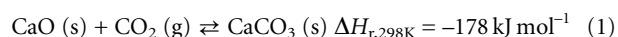
**Keywords:** Calcium looping cycle, CO<sub>2</sub> capture, Nano-sized particles

*Received:* July 02, 2011; *revised:* December 12, 2011; *accepted:* December 19, 2011

**DOI:** 10.1002/ceat.201000299

## 1 Introduction

CO<sub>2</sub> capture and storage technology will be critical for effective mitigation of the climate change in the next few years [1]. There is great interest worldwide in developing large-scale CO<sub>2</sub> capture and sequestration (CCS) technologies. A variety of materials, including hydrotalcite, lithium silicate, MgO, K<sub>2</sub>CO<sub>3</sub>, CaO, etc., are able to absorb CO<sub>2</sub> for large-scale CO<sub>2</sub> capture because of their high reactivity toward CO<sub>2</sub>. A CaO-based sorbent appeared to be thermodynamically the best candidate among metal oxides for conceptual zero-emission power generation systems, all of which involve coal gasification [2]. The CaO-based sorbent, which has rich and extensive resources throughout the world, is currently being widely investigated for CO<sub>2</sub> separation with the following reversible reaction [3–6]:



**Correspondence:** Prof. Y. Zheng (zhengying@mail.hust.edu.cn), Huazhong University of Science and Technology, State Key Laboratory of Coal Combustion, Wuhan 430074, China.

The carbonation reaction is favored when the CO<sub>2</sub> partial pressure in the product gas is higher than the equilibrium partial pressure of CO<sub>2</sub> that results from the decomposition of CaCO<sub>3</sub>. Conversely, CaCO<sub>3</sub> decomposes into CaO when the CO<sub>2</sub> partial pressure in the product gas is lower than the equilibrium partial pressure. The cyclic CO<sub>2</sub> capture processes are high-temperature reactions, typically at 600–950 °C, which can be operated at different pressures. On the one hand, calcium looping has proven to be a promising method of capturing CO<sub>2</sub> in post-combustion technology under atmospheric [7–15] or pressurized conditions [16, 17]. Flue gas CO<sub>2</sub> capture using a calcium looping system is potentially more cost-effective than the traditional amine-based system, whether in a bench-scale test or in an existing power plant [18–20]. On the other hand, calcium looping can be used in advanced hydrogen production systems, such as zero-emission power generation and sorption-enhanced reforming processes [21–26].

Despite the fact that the chemistry of such a calcium looping process is simple, recarbonation is far from being reversible in practice, which is a major challenge for its future application [27–33]. The carbonation reaction is characterized by an initial fast chemical reaction-controlled stage that suddenly changes to a slower diffusion-controlled stage [34]. The sudden transi-

tion results from the formation of a  $\text{CaCO}_3$  layer with a thickness of  $> 50$  nm on the outer surface of the particles. A slow diffusion process governs the progress of the reaction and prevents full CaO conversion on a time scale appropriate for industrial purposes [35]. During long-term cyclic reactions, the proportion of the maximum conversion attributable to the chemical reaction-controlled stage diminishes with the number of calcination-carbonation cycles. One reason of the capture capacity decay of the sorbent is that sintering leads to a change in the CaO particle morphology. Another reason is that the molar volume of the  $\text{CaCO}_3$  formed is much larger than that of CaO, which leads to pore occlusion and an increase in the diffusion resistance of  $\text{CO}_2$  through the carbonation product layer. The available sorbent surface area decreases with the number of cycles, resulting in a low utilization of the sorbent in the long run [36, 37]. Abanades and Alvarez proposed a semi-empirical model to estimate the capture capacity decay of CaO with the number of cycles from a number of CaO-based sorbents as follows [38]:

$$X_{n, \max} = f_m^n (1 - f_w) + f_w \quad (2)$$

They also suggested that the parameters of  $f_m = 0.77$  and  $f_w = 0.17$  are suitable for a wide range of CaO-based sorbents and reaction conditions.

Among the contemporary fields that have experienced impressive advances, nanoscience and nanotechnology are undergoing the most extensive growth. In the early days of the development of calcium looping technology, Baker demonstrated that CaO-based sorbents derived from nano-sized  $\text{CaCO}_3$  ( $\sim 10$  nm) attained a carbonation conversion level constant of 93% after 30 cycles for 24 h of decomposition-back reaction cycles of calcination and carbonation that occurred at  $629^\circ\text{C}$  and  $577^\circ\text{C}$ , respectively [39]. However, the reaction time was too long, and the reaction temperatures were too low to practically representing the cyclic reactivity of nano-sized  $\text{CaCO}_3$ . Florin and Harris studied the properties of CaO-based sorbents derived from nano-sized  $\text{CaCO}_3$  ( $\sim 40$  nm) and found that their  $\text{CO}_2$  capture capability had a high residue of  $\sim 21\%$  after 100-fold 20-min carbonation cycles at  $650^\circ\text{C}$  [36]. They found that the nanostructured sorbent has a higher  $\text{CO}_2$  adsorption ratio due to its higher surface energy.

However, there are few reports describing the characteristics and morphology changes of commercial nano-sized, CaO-based sorbent particles during high-temperature  $\text{CO}_2$  capture cycles, so it is of great importance to conduct further research on the cyclic reaction roles of nano-sized sorbents. The aim of this work is to compare the different characteristics between commercial micro-sized  $\text{CaCO}_3$  and nano-sized  $\text{CaCO}_3$  during calcination-carbonation reactions under the same testing conditions and to attempt investigating the particle morphology changes of two sorbents during high-temperature reactions.

## 2 Materials and Methods

Analytical reagents of micrometer-grade  $\text{CaCO}_3$  with an average particle size of  $35\ \mu\text{m}$  (Shanghai Jing Chun Co. Ltd., Shanghai, China), and nanometer-grade  $\text{CaCO}_3$  with an aver-

age particle size of 40 nm (Chao Dong Group Co. Ltd., Anhui Province, China) were used as precursors of the CaO-based sorbents. The nanometer-grade  $\text{CaCO}_3$  was prepared by high-gravity reactive precipitation [40]. It is worth mentioning that the nanometer-grade  $\text{CaCO}_3$  is a commercial product that can be produced in quantities of more than 100 000 tons per year by Chao Dong Group Co. Ltd. The cyclic calcination-carbonation reactions of the CaO-based sorbents were tested by a tube furnace (Fig. 1). Approximately 2 g of the precursors of the CaO-based sorbents was placed in a quartz sample pan and heated to the calcination temperature of  $850^\circ\text{C}$  at a rate of  $20^\circ\text{C}\ \text{min}^{-1}$  under an  $\text{N}_2$  flow of  $1.5\ \text{L}\ \text{min}^{-1}$  and atmospheric pressure. Once the temperature of  $850^\circ\text{C}$  was reached, it was maintained for 10 min for complete calcination. Then, the gas flow of  $\text{N}_2$  was closed off, while pure  $\text{CO}_2$  at a flow rate of  $1.5\ \text{L}\ \text{min}^{-1}$  under atmospheric pressure was exposed to the carbonate for 30 min. The experimental carbonation temperature and  $\text{CO}_2$  concentration were more extreme than the expected conditions in real capture systems ( $650\text{--}700^\circ\text{C}$ , 15%  $\text{CO}_2$ ), but experimental calcination conditions were milder than those anticipated in a real process ( $900\text{--}950^\circ\text{C}$ ,  $> 90\%$   $\text{CO}_2$ ). The conditions used in this paper have been employed by other authors as effective conditions for calcium looping tests [41, 42].

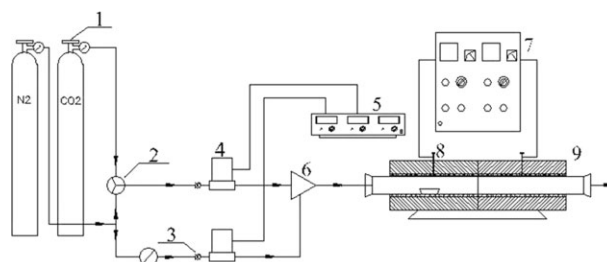


**Figure 1.** Schematic diagram of the tube furnace reaction system. (1) Gas cylinder; (2) valve; (3) filter; (4) flow controller; (5) digital indicator; (6) three-way valve; (7) temperature controller; (8) thermocouple; (9) horizontal tube furnace.

The temperature of the sample was measured by a thermocouple placed outside the tube that was nearest the sample, so the thermocouple touched the tube. A control experiment was performed to monitor the actual temperature by locating a thermocouple inside the tube in which the sample was placed. The reaction gas flow of  $\text{CO}_2$  and  $\text{N}_2$  was controlled by a three-way valve and flow meter controller. The calcined or carbonated samples were moved to the side for cooling in  $\text{N}_2$  and then were removed to be weighed with an electronic balance at room temperature. The carbonation conversion of the samples was calculated as follows:

$$X_n = \frac{m_n - m_0}{m_0} \frac{W_{\text{CaO}}}{W_{\text{CO}_2}} \quad (3)$$

The reaction kinetics of the CaO-based sorbents were investigated in an SAT 409 thermogravimetric analyzer (TGA). Approximately 10 mg of the CaO-based sorbent precursor was placed in a quartz sample pan and heated to the calcination

temperature of 850 °C at a rate of 20 °C min<sup>-1</sup> under an N<sub>2</sub> flow of 30 mL min<sup>-1</sup> and atmospheric pressure. Then, the sample temperature was maintained at 850 °C for 10 min for complete calcination. After calcination, the gas flow of N<sub>2</sub> was closed off and a flow of pure CO<sub>2</sub> of 30 mL min<sup>-1</sup> under atmospheric pressure was exposed to the carbonate for 30 min at 850 °C. The reaction conditions in the TGA were the same as in the tube furnace. The plots of carbonation conversion against reaction time were obtained from the measured weight loss according to Eq. (3). The carbonation rate of each sample was calculated as follows:

$$V_n = \frac{dX_n}{dt} \quad (4)$$

The pore structure parameters of the calcined sample were determined from N<sub>2</sub> adsorption and desorption isotherms, which were measured at the temperature of liquid N<sub>2</sub> (Micromeritics ASAP 2020-M). The surface area and pore volume were calculated from the Brunauer-Emmet-Teller (BET) equations and the Barrett-Joyner-Halenda (BJH) method, respectively. The microstructure of the calcined samples was investigated under high vacuum by field emission scanning electron microscopy (FSEM, SIRION200, FEI Inc.) with 20 kV accelerating voltage. The phase composition of the samples was determined by X-ray diffraction (XRD, PANalytical B.V.) with Cu K $\alpha$  radiation ( $\lambda = 0.1542$  nm) and a  $2\theta$  range of 20–70° with a scanning step of 0.02°. The characteristic peaks of CaO were located at  $2\theta = 32.2, 37.4, 53.9, 64.2,$  and  $67.4^\circ$ . The crystallite sizes and crystal lattice microstrains of CaO-based sorbents were investigated by methods based on Fourier analysis of their XRD peaks using Eqs. (5) and (6), respectively.

$$D = \frac{k\lambda}{\beta \cos \theta} \quad (5)$$

$$\varepsilon = \frac{\beta}{4 \tan \theta} \quad (6)$$

### 3 Results and Discussion

The cyclic carbonation conversions of micro-sized CaCO<sub>3</sub> and nano-sized CaCO<sub>3</sub> in the tube furnace system are presented in Fig. 2. The CaO-based sorbent derived from nano-sized CaCO<sub>3</sub> (NC-CaO) had a higher CO<sub>2</sub> capture capacity than the CaO-based sorbent derived from micro-sized CaCO<sub>3</sub> (MC-CaO) with the same number of cycles. The carbonation conversions after the first cycle for NC-CaO and MC-CaO were 91% and 81%, respectively. However, both samples underwent an unavoidable decay in activity that depended almost solely on the number of calcination-carbonation cycles. The carbonation conversion of NC-CaO remained at 34% after ten cycles, which was 6% higher than that of MC-CaO after ten cycles. This finding means that the activity of the nano-sized sorbent decayed slightly faster compared to that of the micro-sized sorbent under the same conditions. The main reasons for deactivation of the two sorbents were pore occlu-

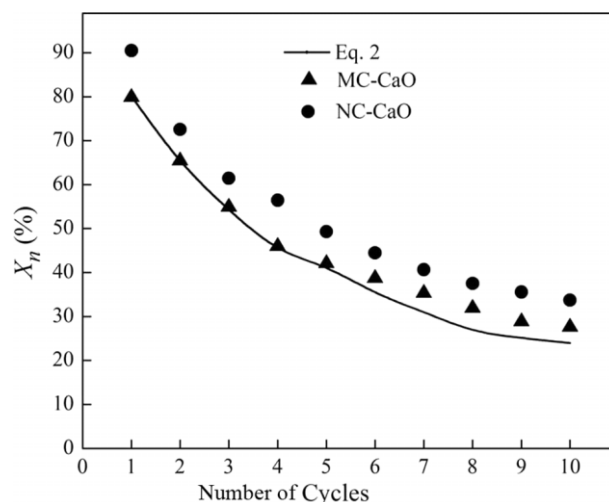


**Figure 2.** Carbonation conversions of MC-CaO and NC-CaO; carbonated at 850 °C in 100% CO<sub>2</sub> for 30 min and calcined at 850 °C in 100% N<sub>2</sub> for 10 min.

sion and an increase in the diffusion resistance of CO<sub>2</sub> through the carbonation product layer, as mentioned previously. It should be noted that Eq. (2) is semiempirical. The rate of sorbent activity decay may fit Eq. (2), but the parameters used in the proposed formulas cannot be easily correlated with the sorbent characteristics. As a result, this equation currently cannot be used to predict the behavior for all of the CaO-based sorbents from their intrinsic properties, especially for the nano-sized sorbent.

Fig. 3 displays the cyclic carbonation kinetics of MC-CaO and NC-CaO with reaction time in the TGA. Whether they were in cycle 1 or in cycle 10, the two sorbents exhibited an exponential increase in the carbonation rate during the initial stage, followed by an abrupt decrease in the carbonation rate. The shift in the reaction mechanism occurred when the small pores were blocked by the formation of a 50-nm-thick nonporous carbonate product layer. As indicated in Fig. 3a, the carbonation conversion of the nano-sized sorbent was nearly at a maximum after 3 min, regardless of the cycle. The carbonation conversions of NC-CaO, after 3 min in cycle 1 and cycle 10, were 73% and 28%, respectively.

Alvarez et al. observed that at the end of the fast chemical reaction-controlled stage, the nonporous CaO particles were marked by the formation of a product layer with a thickness on the order of 50 nm [35]. Therefore, the nano-sized sorbent, with particle or grain sizes of < 100 nm, could be fully carbonated after the chemical reaction-controlled stage. The precursor of the nano-sized sorbent was nanometer-grade CaCO<sub>3</sub> with an average particle size of 40 nm, but the crystallites of the nano-sized particle sintered and agglomerated easily. They were susceptible to merging with larger crystallites (a topic that will be discussed later) during the initial calcination and cyclic high-temperature reactions, which resulted in the continuous growth of particle size. The agglomeration was the primary reason why NC-CaO failed to be fully carbonated after the chemical reaction-controlled stage. In contrast, MC-CaO needed an extended duration for the carbonation process to

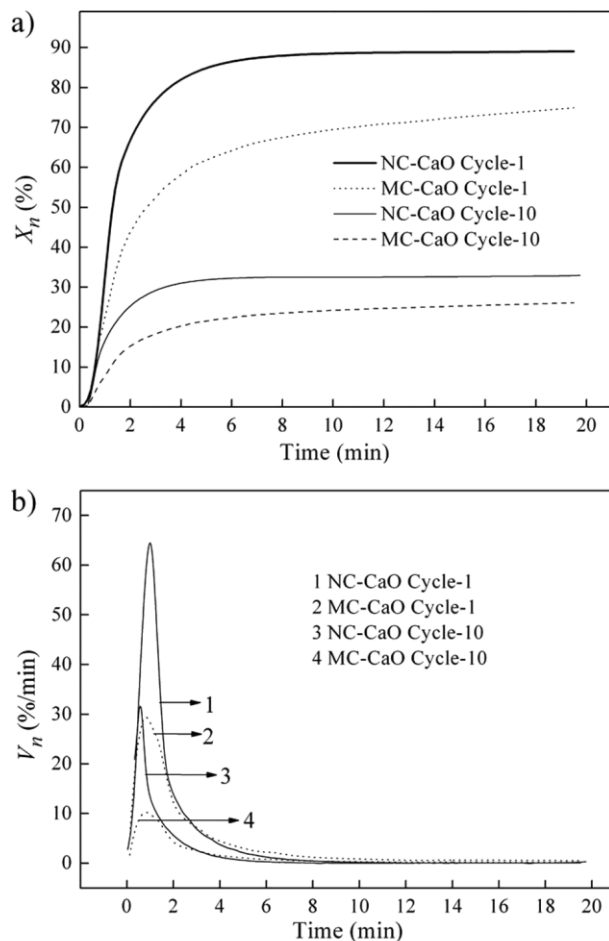


**Figure 3.** Carbonation kinetics of MC-CaO and NC-CaO with reaction time; carbonated at 850 °C in 100% CO<sub>2</sub>. (a) Carbonation conversion vs. time; (b) carbonation rate vs. time.

achieve maximum utilization. The carbonation conversions of MC-CaO after 3 min in cycle 1 and cycle 10 were 49% and 17%, respectively. Fig. 3b reveals that although the proportion of the maximum conversion of NC-CaO decreased after ten cycles, NC-CaO retained its fast carbonation rate at the beginning of each cycle for several tens of seconds. In contrast, the carbonation rate of MC-CaO decreased as the number of cycles increased. Therefore, the nano-sized sorbent was superior to the micro-sized sorbent in terms of carbonation rate during cyclic reactions. Because the reactor design in a calcium looping cycle system is based on the fast reaction regime for carbonation, enhancement of the carbonation rate during long-term reactions is of great significance.

To investigate the crystallite size of CaO-based sorbents in cyclic reactions, all of the calcined NC-CaO and MC-CaO samples from cycle 1 to cycle 5 were characterized by XRD analysis. The mean crystallite size of CaO was roughly estimated using Scherrer's equation. As indicated in Fig. 4, NC-CaO had much smaller crystallite sizes for CaO than for MC-CaO during each cycle. The small crystallite sizes of NC-CaO should be the reason for the fast carbonation rates of the sorbent during each cycle. However, the continuous

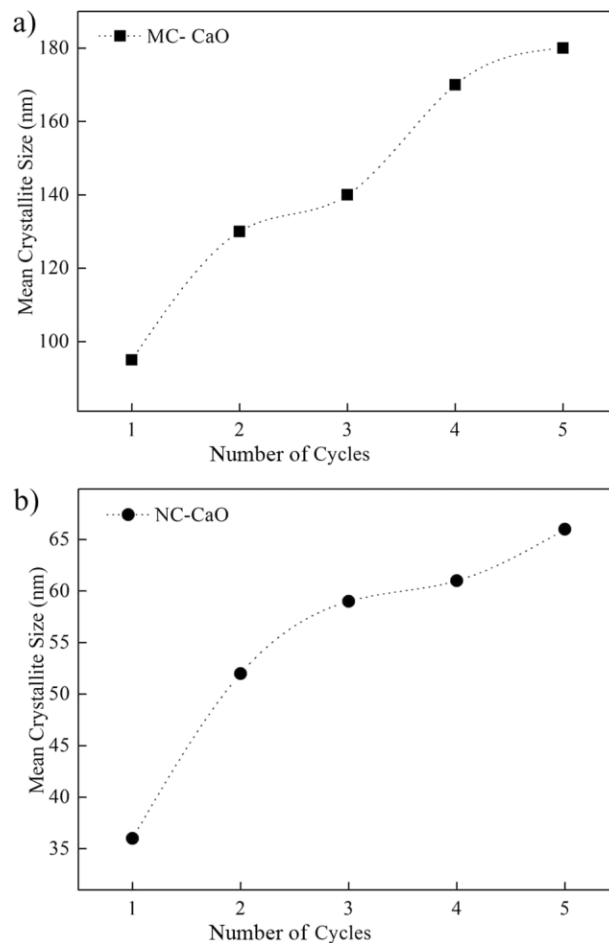


**Figure 4.** Mean crystallite sizes of CaO-based sorbents after calcination during each cycle. (a) MC-CaO; (b) NC-CaO.

increase in crystallite size with the number of cycles (Figs. 4a and b) indicated that both of the sorbents experienced significant sintering during the cyclic reactions.

The BET surface areas presented in Tab. 1 demonstrate that the surface areas of the calcined NC-CaO were larger than those of the calcined MC-CaO before cycle 1 and cycle 10. It is likely that the greater BET surface area of NC-CaO accounted for its superior carbonation behavior. In contrast, BJH pore volume distributions (Fig. 5) proved that the measured pore volumes over the entire range of pore sizes decreased sharply with the number of cycles for MC-CaO and NC-CaO. The different BET surface areas and BJH pore volume distributions of the sorbents were based on their different pore structures, which determined their carbonation performances [34].

**Table 1.** BET surface areas of calcined MC-CaO and NC-CaO before cycle 1 and cycle 10.

Sample	Cycle 1 $S_{\text{BET}}$ [m <sup>2</sup> g <sup>-1</sup> ]	Cycle 10 $S_{\text{BET}}$ [m <sup>2</sup> g <sup>-1</sup> ]
MC-CaO	12.4	2.7
NC-CaO	17.0	3.8

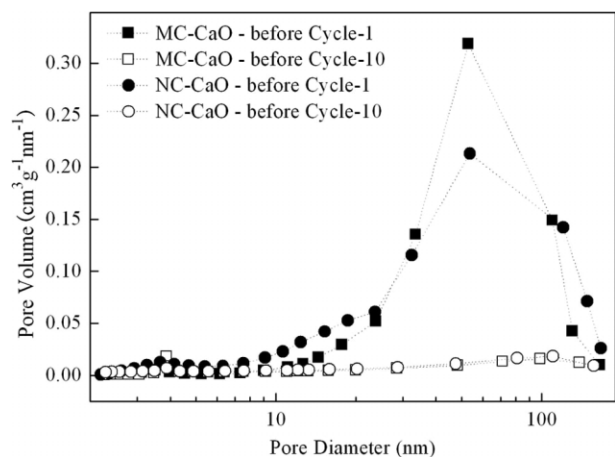


**Figure 5.** BJH pore volume distributions of calcined MC-CaO and NC-CaO before cycle 1 and cycle 10.

An in-depth study of the morphological changes of the micro-sized and nano-sized sorbents during multiple cycles and the determination of the different microscopic characteristics between them will be the subject of further investigations.

Figs. 6 and 7 present FSEM images of the micro-sized and nano-sized sorbents before and after the initial calcination, respectively. The MC grains were composed of cubic microcrystallites (Fig. 6a), which remained after the initial calcination (Fig. 6b). It was also observed that on some broken surfaces of the micro-sized sorbent (Fig. 6c) microcrystallites began to form a rod-shaped arrangement (Fig. 6d) during the

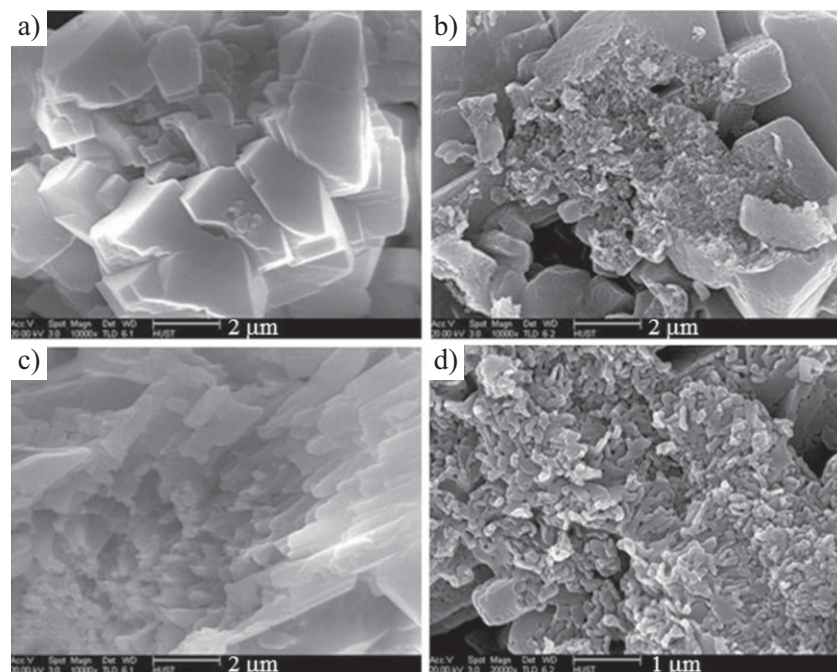


**Figure 6.** FSEM micrographs of micro-sized sorbent. (a), (c) Fresh micro-sized  $\text{CaCO}_3$ ; (b), (d) MC-CaO after initial calcination at  $850^\circ\text{C}$  in  $100\% \text{N}_2$  for 10 min.

initial calcination, which provided a larger specific surface and was beneficial for the later carbonation reaction.

In contrast, NC suffered from dramatic morphological changes after the initial calcination. The NC grains were composed of numerous spherical nanocrystallites (Fig. 7a) and the nano-sized crystallites merged together to form a rough, porous structure (Fig. 7b) after the  $\text{CaCO}_3$  decomposed by releasing  $\text{CO}_2$  during the initial calcination. The smaller size of the crystallites and the porous structure contributed to the BET surface area measured for NC-CaO, which was much larger than that of MC-CaO after the initial calcination. However, the disadvantageous effect of severe sintering among the nanocrystallites began to happen because the agglomeration of nano-sized particles was apparent after the initial calcination.

Fig. 8 presents the FSEM images of calcined MC-CaO and NC-CaO after five calcination-carbonation cycles. Although the morphology of the two sorbents experienced great changes after five cycles, many differences remained between MC-CaO and NC-CaO. As seen in Fig. 8a, there were two different types of textures on the surface of MC-CaO after five cycles. One texture, in which the CaO grains were not fully sintered, was rough and porous. The grains had a rod-shaped arrangement which can also be observed in Fig. 8b. The rough, porous surface of this structure contributed to the rapid chemical reaction-controlled stage during carbonation. The other texture was smooth and usually correlated well with agglomeration. Almost all of the mesopores and macropores were occluded in Fig. 8c and only a few micropores remained on the MC-CaO surface after five cycles. Gupta and Fan proposed that the mesoporous CaO-based sorbent had a better carbonation conversion compared to the microporous CaO-based sorbent [43], thus, the loss of mesopores should have an adverse effect

on the sorbent. In contrast, it can be concluded from Fig. 8d that the size of several particles was  $10\text{--}20\ \mu\text{m}$  after five carbonation-calcination cycles. Therefore, sintering and agglomeration among the nano-sized crystallites seemed to be very severe for this sorbent. There were a few nano-sized crystallites on the surface. The size of some of the crystallites was in the range of  $0.5\text{--}1\ \mu\text{m}$  (Fig. 8e). The micropores on the surface could only be observed at a high magnification (Fig. 8f). It is likely that the nano-sized crystallites merged into larger crystallites during the high-temperature reactions. Therefore, the deactivation of NC-CaO should occur much more quickly than that of MC-CaO during high-temperature  $\text{CO}_2$  capture cycles.

The crystal lattice microstrains of MC-CaO and NC-CaO after calcination in each cycle are depicted in Fig. 9. Microstrain analysis was applied to identify micro-yields at the grain-to-grain interactions resulting from high stress concentrations. Microstrain analysis can also identify macro-yields caused by plastic deformation over the entire sample. The micro-

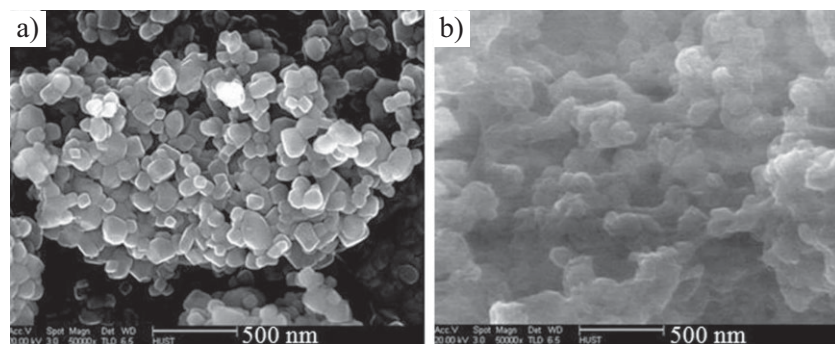


**Figure 7.** FSEM micrographs of nano-sized sorbent. (a) Fresh nano-sized  $\text{CaCO}_3$ ; (b) NC-CaO after initial calcination at  $850\text{ }^\circ\text{C}$  in  $100\% \text{N}_2$  for 10 min.

strain of NC-CaO was approximately two times larger than the microstrain of the MC-CaO in each cycle. It is concluded that the thermal fatigue of the nano-sized CaO grains produced during the long-term, high-temperature reactions should be more severe than that of the micro-sized grains, so the sintering effect is significantly aggravated for NC-CaO.

Based on the experimental evidence presented above, a mechanism of grain boundary migration is reported for aggregation of CaO-based sorbents. The growth of the crystallite is not only the aggregation of the different crystallites, but is also a result of grain boundary migration. As indicated in Fig. 10, the surface of a small crystallite boundary was convex, whereas the surface of a large crystallite boundary was concave. There is a driving force on the crystallite boundary surface caused by a difference in Gibbs free energy that makes the crystallite boundary move towards the center of curvature. As a result,

the smaller crystallites are more susceptible to merging with the larger crystallites during the process of grain boundary migration. As previously demonstrated in Figs. 3, 6, and 7, NC-CaO was composed of numerous spherical nanocrystallites, which were much smaller than those of MC-CaO during each cycle. This resulted in adverse effects to the NC-CaO during long-term, high-temperature reactions.

The results obtained in this paper can potentially be employed for the development of nano-sized, CaO-based sorbents for a calcium looping cycle. Although the nano-sorbent can provide higher carbonation conversions and carbonation rates

during looping cycles, it is imperative that some methods are applied to reduce the grain boundary migration of nano-sized CaO particles to obtain higher conversions and to stabilize the reactivity of the sorbent.

## 4 Conclusions

This study demonstrated that NC-CaO had a higher carbonation conversion and carbonation rate than MC-CaO in cyclic reactions. Furthermore, NC-CaO retained its fast carbonation rate at the beginning of each cycle for several tens of seconds. In contrast, the carbonation rate of MC-CaO diminished with an increase in the cycle number. The measured BET surface areas and pore volumes over the entire pore size range decreased sharply as the cycle number increased for both

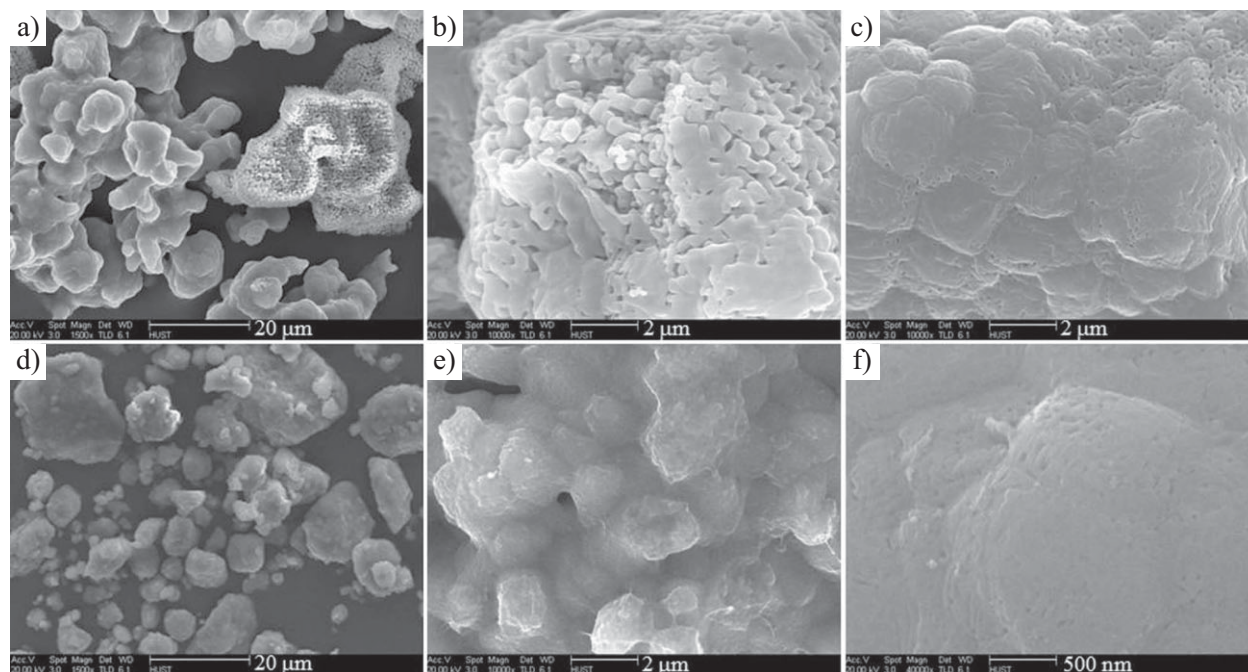


**Figure 8.** FSEM micrographs of the calcined sorbents after five cycles. (a)–(c) MC-CaO; (d)–(f) NC-CaO; each cycle carbonated at  $850\text{ }^\circ\text{C}$  in  $100\% \text{CO}_2$  for 30 min and calcined at  $850\text{ }^\circ\text{C}$  in  $100\% \text{N}_2$  for 10 min.

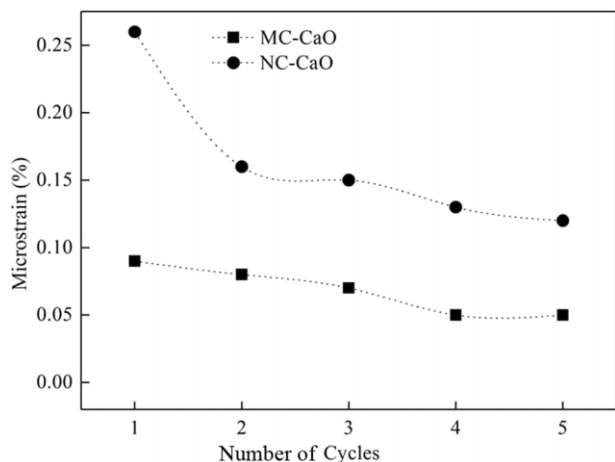


**Figure 9.** Microstrains of MC-CaO and NC-CaO after calcination during each cycle.

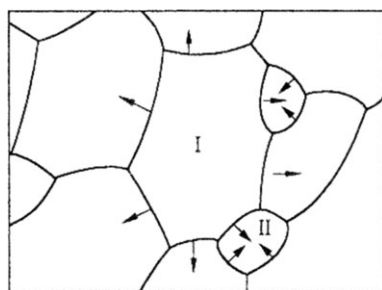


**Figure 10.** Schematic diagram of the CaO grain boundary migration under high-temperature reactions.

NC-CaO and MC-CaO. The BET surface areas of NC-CaO were larger than those of MC-CaO after cycle 1 and cycle 10, resulting in better carbonation rates for NC-CaO during cyclic reactions.

Unfortunately, NC-CaO sintered more easily. Its grains, which were composed of numerous spherical nanocrystallites, suffered from dramatic morphological changes during high-temperature reactions. The microstrain of NC-CaO was approximately two times greater than that of MC-CaO during each cycle. The thermal fatigue of the nano-sized CaO grains produced during the long-term high-temperature reactions were more severe than that of the micro-sized grains, so the sintering effect in cyclic reactions was significantly aggravated for NC-CaO. The growth of the crystallites was not only due to the aggregation of the crystallites, but was also a result of grain boundary migration. The surface of a smaller crystallite boundary was convex, whereas the surface of a larger crystallite boundary was concave. There was a driving force on the crystallite boundary surface that caused a difference in Gibbs free energy and made the crystallite boundary move towards the center of curvature. As a result, the smaller crystallites were more susceptible to merging with the larger crystallites during the process of grain boundary migration.

## Acknowledgment

The authors are grateful for financial supports of the National Basic Research Program of China (No. 2011CB707301), National Natural Science Foundation of China (No. 50936001, 51021065), Doctoral Degree Thesis Innovation Foundation Project of the Huazhong University of Science & Technology (HUST), and Foundation of the China Scholarship Council. The authors also thank the Analytical and Testing Center of HUST for XRD and FSEM measurements.

*The authors have declared no conflict of interest.*

## Symbols used

$D$	[nm]	crystallite size of CaO derived from different sorbents
$f_m$	[-]	constant, = 0.77
$f_w$	[-]	constant, = 0.17
$k$	[-]	Scherrer constant, = 1
$m_n$	[g]	mass of the carbonated sample after $n$ cycles
$m_0$	[g]	mass sample after the initial calcination
$n$	[-]	number of cycle(s)
$t$	[min]	carbonation time
$V_n$	[% min <sup>-1</sup> ]	carbonation rate of the sorbent in cycle $n$
$X_{n,max}$	[%]	maximum carbonation conversion of the sorbent in cycle $n$
$X_n$	[%]	carbonation conversion of the sorbent in cycle $n$
$W_{CaO}$	[g mol <sup>-1</sup> ]	mole mass of CaO
$W_{CO_2}$	[g mol <sup>-1</sup> ]	mole mass of CO <sub>2</sub>

## Greek symbols

$\beta$	[rad]	characteristic peak breadth in XRD spectra
$\varepsilon$	[%]	crystal lattice microstrain of CaO derived from different sorbents
$\theta$	[°]	Bragg angle
$\lambda$	[nm]	X-ray wavelength

## References

- [1] H. Herzog, *Environ. Sci. Technol.* **2001**, *35*, 148A.
- [2] B. Feng, H. An, E. Tan, *Energy Fuels* **2007**, *21*, 426.
- [3] K. O. Albrecht, K. S. Wagenbach, J. A. Satrio, B. H. Shanks, T. D. Wheelock, *Ind. Eng. Chem. Res.* **2008**, *47*, 7841.
- [4] Y. Wu, J. Blamey, E. J. Anthony, P. S. Fennell, *Energy Fuels* **2010**, *24*, 2768.
- [5] Y. Li, C. Zhao, C. Qu, L. Duan, Q. Li, C. Liang, *Chem. Eng. Technol.* **2009**, *32*, 1176.
- [6] Y. Li, C. Zhao, C. Qu, L. Duan, Q. Li, C. Liang, *Chem. Eng. Technol.* **2009**, *32*, 548.
- [7] S. Ramkumar, L. S. Fan, *Ind. Eng. Chem. Res.* **2010**, *49*, 7563.

- [8] Y. Li, C. Zhao, C. Qu, L. Duan, Q. Li, C. Liang, *Chem. Eng. Technol.* **2008**, *31*, 237.
- [9] Z. Yang, M. Zhao, N. H. Florin, A. T. Harris, *Ind. Eng. Chem. Res.* **2009**, *48*, 10765.
- [10] L. Li, D. L. King, Z. M. Nie, C. Howard, *Ind. Eng. Chem. Res.* **2009**, *48*, 10604.
- [11] C. Luo, Y. Zheng, N. Ding, Q. Wu, G. Bian, C. Zheng, *Ind. Eng. Chem. Res.* **2010**, *49*, 11778.
- [12] C. Luo, Y. Zheng, N. Ding, C. Zheng, *Korean J. Chem. Eng.* **2011**, *28*, 1042.
- [13] C. Luo, Y. Zheng, N. Ding, Q. L. Wu, C. Zheng, *Chin. Chem. Lett.* **2011**, *22*, 615.
- [14] K. Wang, X. Guo, P. F. Zhao, C. G. Zheng, *Appl. Clay Sci.* **2010**, *50*, 41.
- [15] B. W. Wang, Y. Zheng, R. Yan, C. G. Zheng, J. G. Shao, J. R. Qiu, *Asia-Pac. J. Chem. Eng.* **2007**, *2*, 197.
- [16] H. C. Chen, C. S. Zhao, Y. J. Li, X. P. Chen, *Energy Fuels* **2010**, *24*, 5751.
- [17] H. C. Chen, C. S. Zhao, L. Duan, C. Liang, D. Liu, X. Chen, *Fuel Process. Technol.* **2011**, 493.
- [18] A. MacKenzie, D. L. Granatstein, E. J. Anthony, J. C. Abanades, *Energy Fuels* **2007**, *21*, 920.
- [19] J. C. Abanades, G. Grasa, M. Alonso, N. Rodriguez, E. J. Anthony, L. M. Romeo, *Environ. Sci. Technol.* **2007**, *41*, 5523.
- [20] Y. Li, C. Zhao, Q. Ren, *Chem. Eng. Technol.* **2011**, *34*, 946.
- [21] B. Feng, W. Q. Liu, X. Li, H. An, *Energy Fuels* **2006**, *20*, 2417.
- [22] W. Q. Liu, B. Feng, Y. Q. Wu, G. X. Wang, J. Barry, J. C. D. da Costa, *Environ. Sci. Technol.* **2010**, *44*, 3093.
- [23] W. Q. Liu, N. W. L. Low, B. Feng, G. X. Wang, J. C. D. da Costa, *Environ. Sci. Technol.* **2010**, *44*, 841.
- [24] J. A. Satrio, B. H. Shanks, T. D. Wheelock, *Ind. Eng. Chem. Res.* **2005**, *44*, 3901.
- [25] K. O. Albrecht, J. A. Satrio, B. H. Shanks, T. D. Wheelock, *Ind. Eng. Chem. Res.* **2010**, *49*, 4091.
- [26] Z. S. Li, N. S. Cai, *Energy Fuels* **2007**, *21*, 2909.
- [27] Z. S. Li, N. S. Cai, Y. Y. Huang, *Ind. Eng. Chem. Res.* **2006**, *45*, 1911.
- [28] H. Lu, A. Khan, S. E. Pratsins, P. G. Smirniotis, *Energy Fuels* **2009**, *23*, 1093.
- [29] V. Manovic, E. J. Anthony, *Ind. Eng. Chem. Res.* **2010**, *49*, 6916.
- [30] R. W. Hughes, A. Macchi, D. Y. Lu, E. J. Anthony, *Chem. Eng. Technol.* **2009**, *32*, 425.
- [31] V. Manovic, E. J. Anthony, *Ind. Eng. Chem. Res.* **2009**, *48*, 8906.
- [32] G. Grasa, J. C. Abanades, E. J. Anthony, *Ind. Eng. Chem. Res.* **2009**, *48*, 9090.
- [33] Y. Li, C. Zhao, H. Chen, C. Liang, L. Duan, W. Zhou, *Fuel* **2009**, *88*, 697.
- [34] H. Lu, P. G. Smirniotis, *Ind. Eng. Chem. Res.* **2009**, *48*, 5454.
- [35] P. G. Alvarez, J. C. Abanades, *Ind. Eng. Chem. Res.* **2005**, *44*, 5608.
- [36] N. H. Florin, A. T. Harris, *Chem. Eng. Sci.* **2009**, *64*, 287.
- [37] P. Sun, J. R. Grace, C. J. Lim, E. J. Anthony, *AIChE J.* **2007**, *53*, 2432.
- [38] J. C. Abanades, D. Alvarez, *Energy Fuels* **2003**, *17*, 308.
- [39] R. Baker, *J. Appl. Chem. Biotechnol.* **1974**, *24*, 221.
- [40] Y. Wang, J. Chen, *China Powder Sci. Technol.* **1998**, *4*, 5.
- [41] P. Sun, J. Lim, J. R. Grace, *AIChE J.* **2008**, *54*, 1668.
- [42] V. Manovic, E. J. Anthony, *Environ. Sci. Technol.* **2009**, *43*, 7117.
- [43] H. Gupta, L.-S. Fan, *Ind. Eng. Chem. Res.* **2002**, *41*, 4035.